Characterization of *iso*-CF_2I_2 in frequency and ultrafast time domains

Patrick Z. El-Khoury,[1] Lisa George,[2] Aimable Kalume,[2] Scott A. Reid,[2,a)] Bruce S. Ault,[3,b)] and Alexander N. Tarnovsky[1,c)]
[1]*Department of Chemistry and Center for Photochemical Sciences, Bowling Green State University, Bowling Green, Ohio 43403-0001, USA*
[2]*Department of Chemistry, Marquette University, Milwaukee, Wisconsin 53201-1881, USA*
[3]*Department of Chemistry, University of Cincinnati, Cincinnati, Ohio 45221-0172, USA*

(Received 24 November 2009; accepted 13 February 2010; published online 22 March 2010)

The photolysis of diiododifluoromethane (CF_2I_2) in condensed phases was studied by a combination of matrix isolation and ultrafast time-resolved spectroscopy, in concert with *ab initio* calculations. Photolysis at wavelengths of 355 or 266 nm of CF_2I_2:Ar samples (1:5000) held at ~8 K yielded *iso*-CF_2I_2 (F_2C-I-I), a metastable isomer of CF_2I_2, characterized here for the first time. The infrared (IR) spectra of this isomer were recorded in matrix experiments, and the derived positions of the C–F stretching modes are in very good agreement with the predictions of high level *ab initio* calculations, which show that the *iso*-form is a minimum on the CF_2I_2 ground state potential energy surface. The formation of this isomer following 350 nm excitation of CF_2I_2 in room temperature CCl_4 solutions was monitored through its intense C–F stretching mode by means of ultrafast time-resolved IR absorption. Together, matrix isolation and ultrafast IR absorption experiments suggest that the formation of *iso*-CF_2I_2 occurs via recombination of CF_2I radical and I atom. Ultrafast IR experiments detect a delayed rise of *iso*-CF_2I-I absorption, placing an upper limit of 400 fs for the C–I bond dissociation and primary geminate recombination processes. The product absorption spectrum recorded 1 ns after 350 nm excitation of CF_2I_2 in solution is virtually identical to the visible absorption spectrum of *iso*-CF_2I_2 trapped in matrix isolation experiments [with subtracted $I_2(X)$ absorption]. The formation of this isomer in solution at room temperature has direct dynamic implications for the ultrafast production of molecular iodine from electronically excited CF_2I_2. © *2010 American Institute of Physics*. [doi:10.1063/1.3357728]

I. INTRODUCTION

Photochemical reaction intermediates are often short lived, surviving on a time scale of a few vibrational periods.[1] They undergo facile intramolecular and intermolecular reactions, and often have unusual geometries and perturbed electronic structures, which in conjunction with their short lifetime, requires multiple experimental and computational approaches to effectively capture and study their properties. There are two general methodologies to study such species that have fleeting existence under normal laboratory conditions. In the first, the intermediates are cooled and trapped in an inert environment, such that their lifetime significantly lengthens and their detection becomes possible with conventional spectroscopic tools—the matrix isolation technique. A second approach is accelerating the experimental detection to allow real-time monitoring of transient species on the femtosecond-to-picosecond time scales with time-resolved spectroscopic techniques. Both approaches have been successfully applied to study short-lived reactive intermediates.

Polyhalomethanes are an important class of compounds that undergo photoinduced bond breaking and structural rearrangement—reactions that have long been of interest to atmospheric and environmental chemistry, photosynthetic chemistry, and chemical reaction dynamics. It was previously demonstrated that condensed phase environments promote a new photochemical path leading to the formation of metastable *iso*-polyhalomethane species.[2–14] The known functions of these reaction intermediates include the production of ions in the ocean[15] and photocyclopropanation reactions of olefins in solution.[16–18] In this regard, one of the most extensively investigated compounds is diiodomethane (CH_2I_2).

Excitation of CH_2I_2 in the gas phase with low-energy photons (<5 eV) causes homolytic cleavage of one of the two C–I bonds on a time scale much shorter than its rotational period,[19,20] with the formation of the iodomethyl radical in high degree of rovibrational excitation.[19] UV excitation of CH_2I_2 in cold N_2 and Ar matrices (12 K) results in the formation of the *iso*-CH_2I_2 form (H_2C-I-I) of CH_2I_2, assigned based on infrared (IR) spectra.[3,4] In a variety of room temperature solutions, this isomer gives rise to an intense UV (~370 nm) and a weaker visible (~530 nm) absorption bands, captured by femtosecond transient absorption spectroscopy.[2,18] This formation of the isomer species in room temperature solutions was confirmed by time-resolved resonance Raman spectroscopy.[5,21] Moreover, time-resolved x-ray diffraction captured the I–I bond length (3.02 Å) for *iso*-CH_2I_2 in methanol. In the case of mixed halogen CH_2BrI and CH_2ClI compounds, *iso*-CH_2BrI and *iso*-CH_2ClI species were reported, which also exhibit dual absorption band spec-

a)Electronic mail: scott.reid@mu.edu.
b)Electronic mail: Bruce.Ault@uc.edu.
c)Electronic mail: atarnov@bgsu.edu.

 © 2010 American Institute of Physics

Downloaded 17 May 2010 to 134.48.30.80. Redistribution subject to AIP license or copyright; see http://jcp.aip.org/jcp/copyright.jsp

tral signatures.[22,23] These isomers possess much shorter lifetimes, 120 ps (Refs. 14 and 21) and 2.5 ns (Ref. 24) for *iso*-CH_2ClI and *iso*-CH_2BrI, respectively. This is in contrast to the long-lived *iso*-CH_2I_2 isomer, which survives on a microsecond time scale in nonpolar and aprotic solvents.[18,25] For other polyhalomethanes, long-lived isomers were captured using transient absorption spectroscopy,[24,26] time-resolved Raman spectroscopy,[9,16,27] and time-resolved x-ray diffraction.[12] To date, the documented intramolecular decay channels of polyhalomethane isomers include homolytic and heterolytic cleavage of a halogen-halogen bond.[18] Bimolecular decay channels in water and alcohol solvents involve an insertion reaction into solvent O–H bonds, leading to the elimination of a dissociative hydrohalogenic acid and hence the formation of halogen ions.[26,28,29]

To build on and expand the studies highlighted above, difluorodiiodomethane (CF_2I_2) serves well as a model system for investigating state selective photochemistry. Excitation of gas-phase CF_2I_2 in the 351–337 nm range exclusively causes direct two-body decay, $CF_2I_2 \rightarrow CF_2I+I$, which occurs much faster than the rotational period of a parent molecule[30] and leads to a high degree of vibrational excitation in the C–I bond of CF_2I.[31] Following excitation of CF_2I_2 into the first excited singlet S_1 state at 350 nm, the quantum yields are 98% and 2% for the $I(^2P_{3/2})$ and $I(^2P_{1/2})$ atoms.[31] Excitation at $\lambda \leq 266$ nm leads to a concerted three-body decay: $CF_2I_2 \rightarrow CF_2+I+I$.[31] In the intermediate range, two-body decay of CF_2I_2 is followed by the C–I bond dissociation in vibrationally hot radicals[30,32] (BDE=12 kcal mol^{-1}).[30] The formation of molecular iodine is observed only upon excitation of CF_2I_2 at 193 nm (6.5 eV).[33–36] In contrast to the gas-phase photochemistry, excitation of CF_2I_2 in *n*-hexane with a single 350 nm photon (3.54 eV) leads to the ultrafast formation of molecular iodine in a 32% quantum yield.[37] Despite the fact that resonance Raman spectra of CF_2I_2 are strongly solvent dependent,[38,39] the several picosecond build up of I_2 was observed in a wide range of solvents (methanol, acetonitrile, linear alkanes, and chlorinated alkanes).[37] Ultrafast formation of I_2 upon excitation of liquid-phase CF_2I_2 is in contrast to the condensed-phase photochemistry of CH_2XI (X=Cl, Br, and I) compounds, where in-cage isomerization is observed and no evidence exists for ultrafast production of molecular halogen products. Moreover, *iso*-CH_2XI intermediates exhibit traceable and characteristic dual absorption bands in the UV-visible spectral range, yet no such bands were observed in irradiated CF_2I_2 solutions.[37] This raises a question of whether or not the photochemical reaction path of CF_2I_2 in solution is entirely different. Mapping the photochemical reaction pathway in S_1 CF_2I_2 showed that an S_1/S_0 conical intersection drives the photochemistry of this molecule from the excited state potential energy surface to a weakly bound ground-state $I\cdots CF_2I$ van der Waals complex, which is thought to be constrained by a solvent cage and subsequently collapses into *iso*-CF_2I_2, an isomer of CF_2I_2.[40] This is consistent with the previous MP2 calculations, which provided computational evidence for the existence of a ground-state potential energy minimum corresponding to *iso*-CF_2I_2.[41] Furthermore, MP2 calculations suggest that the formation of CF_2+I_2 is the lowest energy dissociation channel of *iso*-CF_2I_2, whereas the formation of the CF_2I+I radical pair requires considerably more energy,[41] unlike ground-state *iso*-CH_2I_2.[42] UV excitation of CF_2I_2 leading to vibrationally hot *iso*-CF_2I_2 which rapidly dissociates with the formation of CF_2 and I_2 would account, at least in part, for the observed ultrafast formation of molecular iodine in solution.[41] However, to date the *iso*-CF_2I_2 species was elusive to both trapping and UV/visible/IR detection.

In this work, both general methodologies outlined above, namely matrix isolation and ultrafast spectroscopies, complemented by DFT and *ab initio* calculations, are employed in concert to successfully capture and characterize *iso*-CF_2I_2, an isomer of difluorodiiodomethane.

II. EXPERIMENTAL AND THEORETICAL METHODS

A. Matrix isolation experiments

The matrix isolation experiments utilized a closed cycle two-stage He displex (ARS Displex DE-204S). On the cold tip was mounted a sample holder containing a 25.4 mm diameter CaF_2 window. Initial experiments were done with a CsI cold window; however, once it was determined that IR absorptions of interest were not present below 800 cm^{-1}, a CaF_2 window was used. A loop of 1.0 mm diameter indium wire was used to ensure good thermal contact between the window and sample holder, while a thin layer of cryogenic grease (Apiezon N) was placed between the cold tip and sample mount for the same purpose. A nickel-plated copper radiation shield with two circular ports enclosed the cold tip. The displex and attached radiation shield were inserted into a clamped vacuum shroud, and sealed with a double O-ring seal that allowed the sample assembly to be rotated under vacuum. The vacuum shroud was equipped with four orthogonal window mounts; on two opposing mounts were attached 50.8 mm diameter polished KBr windows. A 10 mm thick custom-made flange that coupled to a commercial pulsed valve (Parker-Hannifin/General Valve Iota-1) was attached to a third mount, orthogonal to the two KBr windows. The pumping station consisted of a liquid-nitrogen trapped diffusion pump (Varian H-4) backed by a scroll pump (Edwards XDS-10), connected to the cryostat via a NW-40 port welded onto the vacuum shroud. An ionization gauge mounted at this port monitored the cryostat pressure. The temperature at the cold tip and sample window were monitored simultaneously using two Si diodes interfaced to a temperature controller (Lakeshore 330). Finally, the entire cryostat was mounted on a homebuilt rail system for quick movement between spectrometers.

IR spectra were obtained with an Fourier transform IR spectrometer (Mattson, Galaxy series) equipped with a Deuterated TriGlycine Sulfate (DTGS) detector, which was purged at a flow rate of 20 l/min using a purge gas generator (Parker-Balston 75–52A). Visible spectra were recorded using a homebuilt spectrometer based on a fiber optic coupled charge-coupled device spectrometer (Control Development). Light from a quartz-tungsten-halogen lamp was directed into a 600 mm fiber (Thorlabs). The fiber output was collimated using an achromatic planoconvex lens and directed onto the sample. The transmitted light was focused into a second

Downloaded 17 May 2010 to 134.48.30.80. Redistribution subject to AIP license or copyright; see http://jcp.aip.org/jcp/copyright.jsp

identical fiber using an identical lens assembly and coupled into the spectrometer. For both IR and visible spectra, reference spectra were recorded for the cold sample holder immediately prior to deposition. IR spectra were recorded at 1 or 2 cm^{-1} resolution and typically averaged over 128 scans. Visible spectra were recorded with a 0.03 s integration time and averaged over typically 500 scans. Several of these were coadded to produce the final spectrum.

The CF_2I_2 sample (Synquest Laboratories, >98.5% purity, used without further purification throughout this work) was placed into a stainless steel bubbler, which in turn was placed into a refrigerated bath (Neslab) held typically at 258 K. The bubbler was pumped under high vacuum for several minutes to remove any volatile impurities, and high purity Ar gas was passed through the bubbler at a typical pressure of 202 kPa, producing a mixture of typically 1500:1 $Ar:CF_2I_2$. This mixture was deposited onto the cold window held at ~8 K using the pulsed deposition technique.[43–46] Typical conditions were as follows: 1 ms pulse duration, 10 Hz repetition rate, and 2 h deposition time.

Following deposition, the cold window was irradiated with 5 ns pulses from a Nd:YAG laser (Continuum Minilite) with a 5 Hz repetition rate; both the Nd:YAG third harmonic (355 nm) and fourth harmonic (266 nm) were used, in separate experiments. The photolysis beam was expanded using a 4:1 beam expander to fill the cold window and avoid damage to the KBr windows. Typical irradiation times were 30 min at 355 nm (6.2 mJ/pulse) and 10 min at 266 nm (2.3 mJ/pulse). Note that the gas-phase absorption cross-section of the parent is around three times larger at 266 nm than at 355 nm.[38] Difference IR spectra of post- and preirradiated matrices were obtained using a subtraction routine in the WINFIRST software package.

B. Time-resolved experiments

The femtosecond transient absorption spectrometer used in this work is based on a 90 fs, 800 nm, 0.92 mJ $pulse^{-1}$ Ti:sapphire regenerative amplifier (Hurricane, Spectra-Physics) pumping two TOPAS-C (Light Conversion Lt.) optical parametric amplifiers.[26,37] Briefly, the amplified 800 nm output is split into two beams of equal intensity. The first beam is delivered to a TOPAS-C "pump" amplifier to produce 350 nm excitation pulses with 6.5 μJ of energy. This beam is focused into a 350 μm spot at the position of the sample (0.25 mm thick jet with a flowing 50 mM solution of CF_2I_2 in CCl_4). The second beam is attenuated and focused onto a 3 mm thick CaF_2 window to produce a white light continuum in the 350–780 nm range, which is split into analyzing/reference probe beams. Transient absorption (ΔA) kinetic traces are measured simultaneously within 274 nm spectral intervals using a spectrograph/dual-diode (analyzing/reference) array detector. Linearity of CF_2I_2 ΔA kinetic traces versus excitation pulse energy is ensured.

For mid-IR probe transient absorption experiments on CF_2I_2 in CCl_4, the excitation energy at the sample position was attenuated to 2 μJ $pulse^{-1}$. The second portion of the 800 nm amplified beam is delivered to a TOPAS-C "probe" amplifier to produce probe pulses covering the 1264–1342 cm^{-1} range. The probe light was split to produce reference and analyzing beams, directed through the sample and subsequently dispersed by an imaging spectrograph (Chromex, 250 is/sm). The signals were read by a 2×32 MCT detector array (Infrared Systems Development Corp.). The calibration of the spectrometer in the investigated spectral region was tested by comparing the positions of the bleaches of an aqueous solution of a reference compound ($[Ru(bpy)_2(dcBpy)Cl_2]$). The femtosecond IR spectrometer has a typical time resolution of about 200–270 fs [full width at half maximum (FWHM)]. This is concluded from Gaussian-like ΔA signals observed at zero time delay between a 350 nm UV-pump and mid-IR probe (1264–1342 cm^{-1}) pulses for neat CCl_4. These features were also used to correct the measured time-resolved IR spectra for chirp (<200 fs in the investigated spectral range). The CF_2I_2 (115 mM) solutions were circulated through a demountable liquid flow cell (DSC-S25, Harrick Scientific) of a 0.25 pathlength with two 2 mm thick BaF_2 windows (REFLEX Analytical Corp.). All time-resolved measurements were performed at magic angle polarization conditions, the pump polarization being set using a Berek compensator to be at 54.7° with respect to the probe polarization.

Nanosecond ΔA measurements were performed on deoxygenated (Ar atmosphere) CF_2I_2 solutions using a combination of a Nd:YAG laser/OPO excitation source (Vibrant LD 355 II, Opotek, 2 mJ $pulse^{-1}$ at 355 nm), a 150 W Xe arc probe lamp (Newport), a Proteus spectrometer (Ultrafast Systems), a monochromator, and a photodiode detector.

CCl_4 (reagent grade, 99.9%) was purchased from Sigma Aldrich. All measurements were performed at room temperature (22 °C).

The SPECTRA-SOLVE™ software package, version 1.5, is employed to fit the mid-IR kinetic traces using a $\Delta A(t) = \Sigma_{i=1}^{4}[A_1 \exp(-t/\tau_i)] + A_5$ function convoluted with the instrument response function (235 fs, FWHM) centered at zero time delay between pump and probe pulses. The reported negative and positive amplitudes represent rise and decay components, respectively, and are normalized such that ΣA_i of the decay component equals 100%.

C. Computational methods

Unconstrained geometry optimization was performed to locate the minima on the CF_2I_2 ground state potential energy surface. All stationary points were characterized by calculating the associated vibrational frequencies. IR intensities for IR active modes are given in parenthesis following the specific vibrational frequency. Geometry optimization was performed using the B3LYP and the more recently developed M06–2X density functionals[47] on one hand, and the MP2 and the coupled-cluster singles and doubles (CCSD) wave functions on the other hand. Two triple zeta quality basis sets are used for the purpose of this study, (i) a small-core relativistic correlation consistent triple zeta valence basis in combination with a pseudopotential to describe iodine atoms (aug-cc-pVTZ-PP),[48] and (ii) the Sadlej-pVTZ (Ref. 49) full atomic basis set with polarization on all atoms. The first

Downloaded 17 May 2010 to 134.48.30.80. Redistribution subject to AIP license or copyright; see http://jcp.aip.org/jcp/copyright.jsp

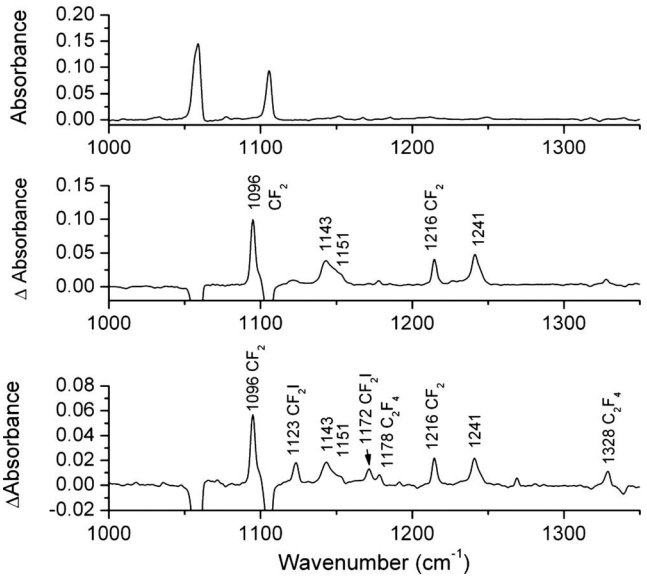

FIG. 1. Upper panel: IR spectrum of a CF_2I_2:Ar matrix (1:1500) at 8.5 K in the C–F stretching region. Middle panel: Difference spectrum obtained following irradiation of an as-deposited matrix at 355 nm (details in the text). Lower panel: Difference spectrum obtained following irradiation of an as-deposited matrix at 266 nm (details in the text).

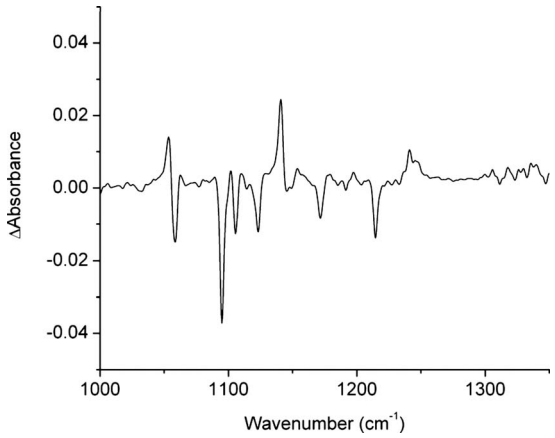

FIG. 2. Difference spectrum obtained following annealing of a CF_2I_2:Ar matrix (1:1500) that was first irradiated at 266 nm. Details are provided in the text.

basis sets recovers some of the correlation energy of the valence electrons, an important feature in describing weak bonding situations such as the molecules examined here. The second basis set, parameterized to recover electrostatic properties, has been found to predict accurate vibrational frequencies for structurally related molecules. The aug-cc-pVXZ-PP series (where X=D, T, and Q) which constitute a logical sequence of basis sets that converge toward the basis set limit were tested, and it has been found that the geometrical parameters are almost converged with respect to a further increase in basis set description (from a triple ζ to a quadruple ζ quality basis set). All angles are reported in degrees and bond lengths in angstroms. These calculations were performed using the methodologies developed in the GAUSSIAN 09 program.[50]

III. RESULTS AND DISCUSSION

We begin by discussing the matrix isolation experiments. Figure 1 shows IR spectra in the C–F stretching region for an as-deposited Ar:CF_2I_2 ($\sim$1:1500) matrix (upper panel), a difference spectrum following 355 nm irradiation of a freshly deposited matrix (middle panel), and a difference spectrum following 266 nm irradiation of a freshly deposited matrix (lower panel). The as-deposited sample contains two prominent features at 1058 and 1105 cm^{-1}, readily assigned to the parent CF_2I_2 C–F stretching modes. The frequencies are in very good agreement with theoretical expectations: B3LYP/Sadlej-pVTZ (1059, 1102 cm^{-1}), MP2/Sadlej-pVTZ (1058, 1104 cm^{-1}). Upon irradiation at 355 or 266 nm, the parent bands decrease and prominent absorptions due to $:CF_2$ are apparent, with new bands also observed at 1143, 1151 cm^{-1} (shoulder on the 1143 cm^{-1} absorption), and 1241 cm^{-1}.[51,52] In addition, upon 266 nm irradiation, bands assigned to the CF_2I radical are clearly observed at 626, 1123, and 1172 cm^{-1}. The 1172 cm^{-1} band has not previously been reported but can be assigned to CF_2I.[53]

To investigate the origin of the unassigned (1143, 1151, and 1241 cm^{-1}) absorptions, we annealed the irradiated matrices. Figure 2 displays a difference spectrum (post-versus preannealing) for annealing a matrix that was first irradiated at 266 nm. The annealing protocol involved heating the matrix to 33 K, holding this temperature for 20 min, and recooling to 8.5 K. As expected, the radical ($:CF_2$, CF_2I) absorptions decrease upon annealing, while the 1143 cm^{-1} and 1241 cm^{-1} bands are the only absorptions which significantly *increase*. Note that in this spectrum a band close to the 1058 cm^{-1} absorption of the parent CF_2I_2 also increases; however, this reflects changes in the spectrum of the unphotolyzed parent upon annealing, which was confirmed by annealing a freshly deposited CF_2I_2 matrix, the spectrum of which displayed a very similar pattern (Fig. S1, supplementary information[54]). Although not shown here, similar results (decrease in $:CF_2$ absorptions, increase in the 1143 and 1241 cm^{-1} bands) were obtained when annealing a matrix that had first been irradiated at 355 nm.

The annealing experiments give several important insights. First, they suggest that the 1143 and 1241 cm^{-1} bands belong to a common species. Second, the increase of these bands upon annealing suggests that this species is not a radical intermediate. Finally, the annealing experiments show that, while $:CF_2$ absorptions decrease in intensity, bands associated with C_2F_4 do not increase, indicating that $:CF_2$ is recombining with I_2 (or I) in the matrix cage. The formation of the parent CF_2I_2 isomer from the recombination of $:CF_2$ and I_2 is not favored at low temperature, as a sizable (18.8 kcal mol^{-1}) barrier exists to insertion of the carbene into the I–I bond.[41] In contrast, the formation of the *iso*-CF_2I_2 form (i.e., F_2C–I–I) is an exothermic barrierless process, and is therefore favored in the matrix. Considering the weight of available evidence, we assign the 1143 and 1241 cm^{-1} bands to the asymmetric and symmetric C–F stretching modes of *iso*-CF_2I_2, respectively. The 1151 cm^{-1} band represents a site splitting [inferred from Ne matrix (5

Downloaded 17 May 2010 to 134.48.30.80. Redistribution subject to AIP license or copyright; see http://jcp.aip.org/jcp/copyright.jsp

TABLE I. Calculated vibrational frequencies (cm^{-1}) for CF_2I_2 at various levels of theory.

	B3LYP		M06–2x		MP2	
Method	aug-cc-pvtz-PP	Sadlej-pVTZ	aug-cc-pvtz-PP	Sadlej-pVTZ	aug-cc-pvtz-PP	Sadlej-pVTZ
ν_1	109 (0)	111 (0)	118 (0)	119 (0)	117 (0)	119 (0)
ν_2	245 (0)	249 (0)	252 (0)	257 (0)	253 (0)	255 (0)
ν_3	267 (0)	268 (0)	281 (0)	283 (0)	286 (0)	283 (0)
ν_4	270 (0)	272 (0)	283 (0)	283 (0)	289 (0)	285 (0)
ν_5	304 (0)	308 (0)	319 (0)	321 (0)	316 (0)	315 (0)
ν_6	603 (5)	600 (5)	617 (5)	615 (5)	605 (4)	595 (4)
ν_7	725 (345)	726 (338)	764 (337)	762 (329)	779 (299)	759 (317)
ν_8	1064 (279)	1060 (270)	1118 (279)	1111 (267)	1081 (250)	1059 (251)
ν_9	1106 (141)	1104 (141)	1179 (140)	1177 (139)	1124 (128)	1104 (132)

K) experiments, Fig. S2 (Ref. 54)]. To investigate this further and put our assignments on stronger footing, we carried out (a) extensive *ab initio* studies of this system and (b) time resolved ultrafast IR spectroscopy of CF_2I_2 in the solution phase.

With few exceptions, the method of choice for computing the electronic structures and electronic/vibrational spectra of small halogenated alkanes and their various photochemical reaction products is the B3LYP density functional and its time-dependant analog, due to a reduced computational cost with a reasonably acceptable error bar that varies from one case to another.[37,38,55–62] This method and others were used to optimize the geometrical parameters of the CF_2I_2 parent structure (Table S1, supplementary information[54]). The calculated structure of CF_2I_2 is not sensitive to either the choice of basis set, or the fundamentally different wave functions and density functionals tested. Since the predicted geometries are fairly similar within a tight error bar, the parent molecule was used to test the performance of different methods in combination with two different basis sets (aug-cc-pVTZ-PP and Sadlej-pVTZ) in predicting vibrational frequencies. The computed vibrational frequencies are shown in Table I. The two fundamental vibrations of particular interest are ν_8 and ν_9, the C–F stretching modes. The B3LYP/aug-cc-pvtz-PP, B3LYP/Sadlej-pVTZ, and MP2/Sadlej-pVTZ calculated frequencies are self-consistent, and agree well with experiment (Fig. 1). However, the MP2/aug-cc-pVTZ frequencies are slightly overestimated by factors of 1.02 for both ν_8 and ν_9. The M06–2x/aug-cc-pVTZ and M06–2x/Sadlej-pVTZ on the other hand are significantly overestimated: factors of 1.06/1.07 for ν_8/ν_9 using the correlation consistent basis set, and factors of 1.05/1.07 for ν_8/ν_9 when the Sadlej-pVTZ basis set is used.

The fully optimized geometrical parameters of *iso*-CF_2I_2 (i.e., F_2C-I-I) at various levels of theory are given in Table II. Within the same method, the computed geometrical parameters are not sensitive to the choice of basis set. However, when different functionals/wave functions are compared, the B3LYP functional underestimates the values of the C–I bond and the C–I–I angle when compared to all other methods used in this work. Judging from the CCSD results, the predicted B3LYP geometrical parameters seem to be in error. We attribute the differences to a poor performance of the B3LYP functional in describing the weakly bound F_2C-I-I structure. This is corrected for by electron correlation in wave function methods, and double the amount of non-local exchange in the case of the M06–2X functional.[47] A nearly linear F_2C-I-I isomer structure is predicted using the MP2 and CCSD methods (a C–I–I angle of 180° in both cases). In this case, the relatively "cheap" M06–2x and MP2 computed structures are fairly close to its "expensive" CCSD analogs. The calculated fundamental vibrational frequencies for the F_2C-I-I isomer structure are shown in Table III. Since the B3LYP structure is in error, the associated vibrational frequencies are disregarded. The fundamental vibrational frequencies of interest (captured in the matrix) are ν_8

TABLE II. Optimized structural parameters for *iso*-CF_2I_2 at various levels of theory.

Method	C–F	C–I	I–I	F–C–F	F–C–I	C–I–I
B3LYP/						
aug-cc-pvtz-PP	1.295	2.570	2.780	106.9	121.7	166.9
Sadlej-pVTZ	1.298	2.678	2.785	106.6	122.0	168.3
M06–2x/						
aug-cc-pvtz-PP	1.287	3.043	2.678	105.6	127.0	176.4
Sadlej-pVTZ	1.291	3.127	2.676	105.4	126.9	176.3
MP2/						
aug-cc-pvtz-PP	1.291	2.835	2.695	106.2	126.9	180.0
Sadlej-pVTZ	1.303	3.046	2.702	105.6	127.2	180.0
CCSD/						
aug-cc-pvtz-PP	1.290	3.054	2.697	105.6	127.2	180.0
Sadlej-pVTZ	1.306	2.954	2.779	106.1	127.1	180.0

Downloaded 17 May 2010 to 134.48.30.80. Redistribution subject to AIP license or copyright; see http://jcp.aip.org/jcp/copyright.jsp

TABLE III. Calculated vibrational frequencies (cm^{-1}) for *iso*-CF_2I_2 at various levels of theory.

	B3LYP		M06–2x		MP2			
Method	aug-cc-pvtz-PP	Sadlej-pVTZ	aug-cc-pvtz-PP	Sadlej-pVTZ	aug-cc-pvtz-PP	Sadlej-pVTZ	Sym.	Assignments[a]
ν_1	26 (0)	24 (0)	12 (0)	12 (0)	22 (0)	19 (0)	A'	C–I–I bend out-of-plane
ν_2	57 (0)	51 (0)	24 (0)	27 (0)	27 (0)	20 (0)	A''	C–I–I bend in-plane
ν_3	77 (16)	71 (13)	64 (6)	60 (5)	67 (14)	55 (7)	A'	C–I stretch
ν_4	152 (0)	136 (0)	78 (0)	74 (0)	105 (0)	81 (0)	A''	CF_2 rock
ν_5	172 (13)	175 (13)	187 (2)	185 (3)	202 (0)	160 (0)	A'	CF_2 wag
ν_6	325 (51)	290 (44)	223 (7)	223 (5)	212 (10)	216 (5)	A'	I–I stretch
ν_7	668 (5)	667 (5)	695 (5)	693 (5)	682 (2)	670 (2)	A'	CF_2 scissor
ν_8	1183 (303)	1181 (307)	1220 (246)	1215 (348)	1199 (348)	1154 (362)	A''	CF_2 asym. str.
ν_9	1218 (709)	1223 (636)	1303 (323)	1300 (301)	1282 (291)	1252 (260)	A'	CF_2 sym. str.

[a]Tentative assignments based on the calculated MP2/Sadlej-pVTZ vibrational frequencies.

and ν_9, assigned to the C–F stretching modes at the CF_2 moiety in the F_2C-I-I isomer. When the scaling factors derived from the parent molecule are applied for both M06–2x and the MP2/aug-cc-pVTZ calculated frequencies, the resulting computed frequencies are self-consistent within an acceptable error bar. However, this approach is over simplistic in nature as it presupposes the same electronic environment around the two C–F anharmonic oscillators, and it will not be discussed further. Without applying any scaling factors, the MP2/Sadlej-pVTZ frequencies can be directly assigned to the observed 1143/1151 and 1241 cm^{-1} vibrational signatures due to the F_2C-I-I isomer captured in the matrix.

To understand why an accurate description of the minimum requires highly correlated electronic structure methods, a two-dimensional (2D) relaxed redundant coordinate scan around the isomer minimum was performed at the MP2/Sadlej-pVTZ level of theory along the C–I–I angle and C–I bond. The MP2 and CCSD wave functions favor a linear geometry for the isomer minimum, Fig. 3. However, the potential energy surface in the vicinity of MP2/CCSD global minimum is shallow enough for the constrained parameters corresponding to the optimized B3LYP geometry to lie within a barrierless 3 kcal/mol from the critical point. The shallowness of this part of the isomer ground state potential energy surface indicates that multiple conformations are accessible within a few kcal/mol, the calculated zero point energy of the MP2 fully optimized minimum being about 5 kcal/mol.

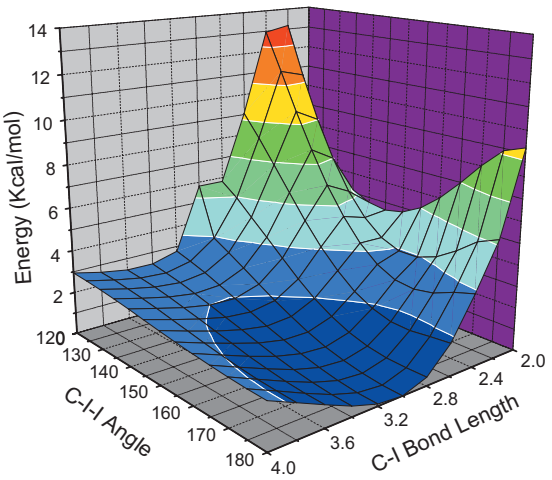

FIG. 3. Calculated (MP2/Sadlej-pVTZ) potential energy surface of CF_2I_2 in the region of the *iso*-CF_2I_2 minimum. This surface represents a relaxed 2D scan along the C–I–I angle and C–I bond distance.

The dynamics of the *iso*-CF_2I_2 isomer formation in liquid solutions at ambient temperatures is investigated by means of ultrafast 350 nm pump/mid-IR absorption probe technique, which probes *iso*-CF_2I_2 through the high-energy wing of its intense and broad absorption band due to symmetric C–F stretch (1241 cm^{-1} in the matrix, υ_9 = 1252 cm^{-1} calculated, Table III). The 1265 and 1319 cm^{-1} kinetic ΔA traces recorded during the first 50 ps after UV-pulse excitation, the best multiexponential fits (convoluted with the instrument response function, 235 FWHM), and time-resolved IR spectra are illustrated in Fig. 4. Between −400 and 400 fs, the ΔA transient absorption signal has contributions both from the solute and solvent. The ΔA signal for the neat CCl_4 solvent was measured at identical conditions immediately before and after the CF_2I_2/CCl_4 experiment. The solvent does not exhibit noticeable transient absorption at time delays longer than 400 fs. The presence of the similarly shaped negative signals at negative time delays (~−200 fs) in both CF_2I_2/CCl_4 and neat CCl_4 kinetic traces permitted the scaling (x ~ 0.22) and subsequent subtraction of the neat solvent signal from the total ΔA signal.

A delayed sub-1-ps rise is noticeable in the total ΔA signal, but it is especially prominent after solvent subtraction. A broad absorption tailing from 1264 to 1342 cm^{-1} dominates at short time delays between 0.1 and 1 ps. Following a delayed sub-1-ps rise, the transient absorption exhibits a pronounced decay on a time scale of a few picoseconds. The fast rise is more pronounced at smaller probe frequencies. From 0.5 to 5 ps kinetics traces within the investigated spectral range are perfectly superimposable. However, at 5 ps, a noticeable spectral narrowing toward the low energy wing is observed, with transient absorption shaping below 1270 cm^{-1}. Between 5 and 20 ps, the ΔA signal exhibits some recovery that is more pronounced in the high-energy part of the spectrum, which is followed by decay on a time

Downloaded 17 May 2010 to 134.48.30.80. Redistribution subject to AIP license or copyright; see http://jcp.aip.org/jcp/copyright.jsp

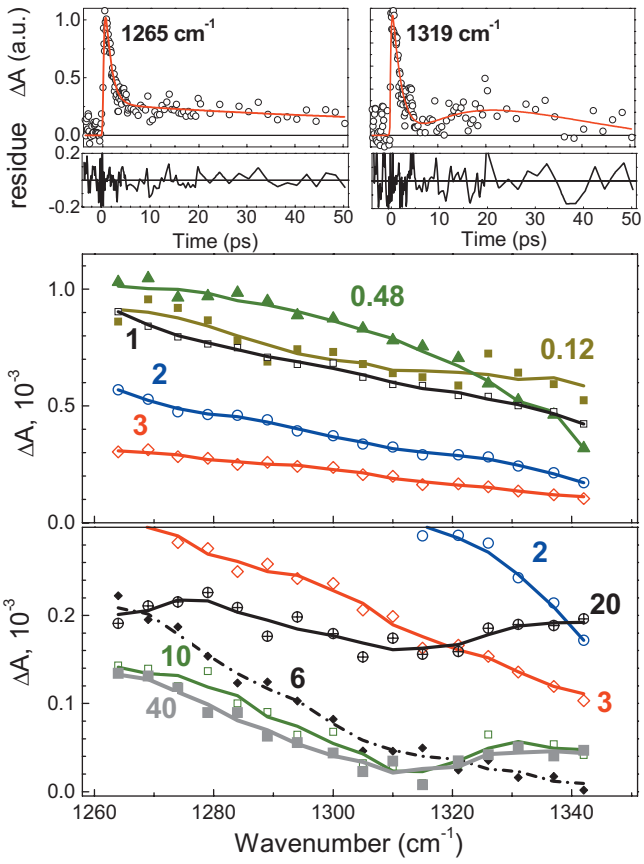

FIG. 4. Time resolved mid-IR spectra following 350 nm excitation of CF_2I_2 in CCl_4. Upper panels: The 1265 and 1319 cm^{-1} kinetic ΔA traces (symbols) superimposed on their best multiexponential fits (lines, convoluted with an instrument response function of 235 fs, FWHM). The fit residuals are also shown. Lower panels: the evolution of transient absorption ΔA spectra at selected time delays between UV-pump and IR-probe pulses. Time delays (in picoseconds) are indicated next to the individual spectra. Symbols represent measured data points where lines represent smoothed (3pts, adjacent averaging) data to guide the reader's eye.

scale of several tens of picoseconds. The resulting ΔA signal (50 ps) resembles that observed at 5 ps, and consists of a small residual tail indicative of product absorption band maximum centered at a lower energy then 1264 cm^{-1}. The spectral fit of the residual 50 ps ΔA spectrum to a Gaussian function predicts an IR absorption line shape centered at $\sim$1255 cm^{-1} with a FWHM of $\sim$70 cm^{-1}.

The best-fit time constants describing the evolution of the transient absorption are 0.35 ± 0.15 ps (τ_1, major rise, amplitude A_1), 1.2 ± 0.4 ps (τ_2, major decay, amplitude A_2), two several tens of picoseconds time constants ($\tau_3 = 13 \pm 3$ ps and $\tau_4 = 26 \pm 4$ ps), which appear as a rise and a decay, respectively, and have more pronounced amplitudes ($A_{3,4}$) at the high-energy wing of the spectrum, as well as a persistent offset (amplitude A_5). Specifically, the 1265 cm^{-1} ΔA signal can be characterized by the following components: $\tau_1 = 0.3$ ps ($A_1 = -100\%$), $\tau_2 = 1.5$ ps ($A_2 = 71\%$), $\tau_3 = 12$ ps ($A_3 = -23\%$), $\tau_4 = 25$ ps ($A_4 = 21\%$), and $A_5 = 8\%$, whereas the 1319 cm^{-1} ΔA signal can be characterized by the following components $\tau_1 = 0.3$ ps ($A_1 = -68\%$), $\tau_2 = 1.5$ ps ($A_2 = 47\%$), $\tau_3 = 12$ ps ($A_3 = -50\%$), and $\tau_4 = 25$ ps ($A_4 = 53\%$), upper panels of Fig. 4. In contrast to the best fits, note that the ΔA spectra are reconstructed from the ΔA kinetic traces, and therefore tend to exhibit more pronounced point-to-point deviations when selected spectra at different time delays are compared. Nevertheless, similar time constants are obtained from frequency-integrated time-resolved IR spectra.

According to theoretical predictions and the results from matrix isolation, the CF_2I_2 parent and CF_2I radical species do not absorb above 1200 cm^{-1}, and therefore the IR absorption signal in the probed spectral range can only be due to the *iso*-CF_2I_2 species. However, the possibility of a contribution from isomerlike distorted transient structures/intermediates cannot be ruled out, especially at short delay times. Following photodissociation, considerable excess of energy is available to the CF_2I photofragment,[30,31] which probably emerges as rovibrational excitation as in the $CH_2I_2 \rightarrow CH_2I + I$ photodissociation,[19] based on the strong structural similarly between CH_2I_2 and CF_2I_2 and similarly highly vibrationally excited C–I bonds observed in both polyatomic photofragments.[19,31] Somewhat less excess of energy is available to the isomer species produced by primary geminate recombination. Therefore, the assignment of the temporal evolution of the observed IR ΔA is complicated by contributions from both population and vibrational relaxation, namely, intramolecular vibrational redistribution (IVR) and intermolecular energy transfer to the solvent (IET). If one assumes a conventional hierarchical mechanism of vibrational relaxation, IVR is followed by IET.[63–66] Vibrational cooling typically takes place on time scales of several tens of picoseconds.[65,66] For a structurally related CH_2I_2/CCl_4 system, vibrational cooling time constants were reported to be between 70–87 ps following excitation into the C–H stretch and its first overtone,[67,68] and 107–117 ps for excitation into a C–H stretch and H–C–H bend combination mode.[68–70] Therefore, the fast appearance of the IR absorption (time constant, τ_1) can be attributed to the isomer product formation convoluted with IVR. As the primary photochemical event is the breaking of a C–I bond in CF_2I_2,[40] the observed ultrafast time constant defines an upper limit of 400 fs for primary geminate recombination to form *iso*-CF_2I_2.

The nascent isomer contains internal energy excess, and the short-time (0.1–1 ps) IR signal in the isomer C–F moiety is spectrally broad, exhibiting a fast rise that is prominent in the region of the metastable IR band ($\sim$1260 cm^{-1}) but less pronounced in the high-energy wing. Significant intensity in the high-energy wing of the C–F absorption band at short times may arise as a result of initial population of low frequency modes, mostly of bending and deformational nature in the case of *iso*-CF_2I_2, which give rise to positive anharmonic coupling terms.[71–75] On this short-time scale, the IR signal undergoes significant spectral changes, without showing any negative contribution due to stimulated emission. These observations are consistent with the formation of the *iso*-CF_2I_2 isomer in a nonequilibrated population distribution (without population inversion) in the C–F mode. In addition, the shallowness of the ground state potential in the vicinity of the isomer minimum implies that a broad distribution of isomer transient structures is accessible and hence probed at short time delays. Together, these arguments suggest that the short-time C–F lineshape is inhomogeneously broadened. Because of the shallowness of the ground state potential, the

Downloaded 17 May 2010 to 134.48.30.80. Redistribution subject to AIP license or copyright; see http://jcp.aip.org/jcp/copyright.jsp

structural inhomogeneity is most likely preserved following the completion of vibrational relaxation processes. Although convoluted population and vibrational dynamics dominates the short time spectra (0.1–0.5 ps), it is population relaxation that governs the several picosecond time scale as evidenced by superimposable kinetics traces from 0.5 to 5 ps.

We note that the calculated symmetric C–F stretching vibrational frequency of *iso*-CF_2I_2 is approximately equal (within ~100 cm^{-1}) to twice the calculated υ_7 fundamental vibration, Table III. Therefore, the isomer species appears to have a built-in intramolecular vibrational energy deactivation pathway which channels one quantum deposited on the CF_2 moiety into two quanta of the υ_7 fundamental vibration. In the widely accepted tier model, an interaction between vibrational eigenstates is stronger for lower-order couplings.[63,76] A low-order tier (second order, 1250 $cm^{-1}=2\times670$ cm^{-1} +90 cm^{-1}, where 90 cm^{-1} is within the phonon bandwidth of about 200 cm^{-1} in molecular liquids,[76,77] supplied by a dynamically fluctuating solvent medium) accounts for fast intramolecular vibrational energy transfer out of the CF_2 moiety into the overtone of ν_7. This mode (ν_7) is best described by CF_2 scissoring coupled to C–I stretching. The C–F absorption significantly weakens toward 5 ps. This process precedes (or, accompanies) the ultrafast formation of I_2 observed in the previously reported 350 nm pump/visible probe experiments.[37] These observations strongly suggest that (i) the depopulation of ν_9 and population of ν_7 opens a pathway for the dissociation of *iso*-CF_2I_2 into CF_2+I_2, and (ii) the excess vibrational energy is redirected into the "reactive" C–I mode in *iso*-CF_2I_2 on an ultrafast (1–2 ps) time scale, Fig. 4.

As early as 5 ps, a clear indication of a low-energy absorption band is observed. The subsequent rise and decay of the absorption between 10 and 40 ps—also observed in the frequency-integrated time-resolved ΔA spectra—corresponds to a second phase of population of the C–F symmetric stretch in the isomer species. This phase occurs on a timescale characteristic of heavy-solvent translation motion, the end of IVR, altogether with the onset of vibrational cooling. The tens of picosecond time scale observed can be attributed to a second phase in the isomer formation and may involve local solvent reorganization and partially thermalized CF_2I radical species. A noticeable offset of transient absorption kinetics at 50 ps time delay manifests that some isomer species survive to be present on longer time scales (hundreds of picoseconds). These species are trapped in cold matrices as discussed above and observed on a sub-nanosecond time scale in 350-pump/visible-probe femtosecond pump probe, as discussed below.

The electronic spectrum of matrix-isolated *iso*-CF_2I_2 was also recorded. The difference spectrum of a CF_2I_2:Ar (1:1500) matrix before and after irradiation at 355 nm is shown in Fig. 5, panel A. Clear absorption signatures are observed in the 400–550 nm region. Recall that the only IR absorptions observed to increase following 355 nm irradiation belong to *iso*-CF_2I_2 and: CF_2 (Fig. 1). The observation of the latter and the change in color of the matrix upon irradiation suggest that I_2 is also formed, and this is responsible for the broad feature at ~520 nm. We note that :CF_2 has a

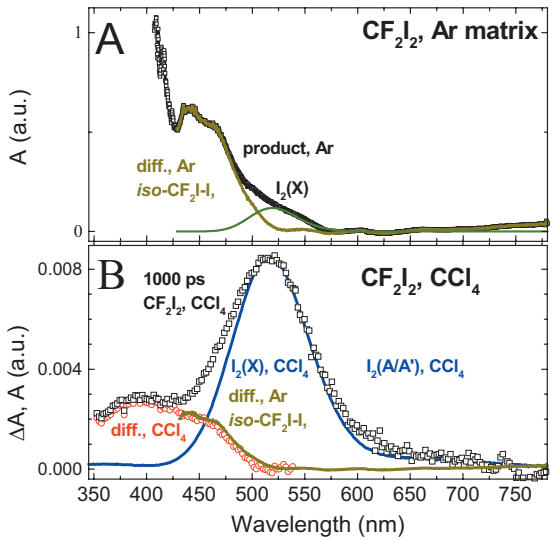

FIG. 5. Panel A. Visible absorption spectrum of CF_2I_2 in an Ar matrix after irradiation at 355 nm before (symbols) and after (thick line) subtraction of the steady-state absorption of I_2 (thin line). The contribution of the I_2 species to the total product absorption was obtained by deconvoluting the spectrum into three Gaussian bands (with I_2 absorption centered at 519 nm (Ref. 78). Panel B. Transient absorption ΔA spectrum measured 1 ns after 350 nm excitation of CF_2I_2 (50 mM) in CCl_4 (black symbols) is overlapped with the steady-state absorption spectrum of molecular iodine in the same solvent (518 nm maximum, thick blue line). Subtracting the I_2 spectrum from the ΔA spectrum yields "I_2-free" product spectrum (open circles), superimposable on the matrix-isolated absorption spectrum of the *iso*-CF_2I–I species in the 430–530 nm range obtained in Panel A. The minor deviation in the red spectral range is due to I_2 absorption from excited A/A' states.

known visible spectrum corresponding to the S_0-T_1 transition, which has been observed in emission;[79,80] however, this system is very weak and should not contribute to the spectrum in Fig. 5. Therefore, we assign the broad features observed between 400 and 500 nm to the *iso*-CF_2I_2 product species. An estimate for the maximum molecular decadic extinction coefficient (ε_{max}) for *iso*-CF_2I_2 in the visible range can be obtained by using the calculated IR (ν_9) intensities and measured IR spectrum (around the 1241 cm^{-1} feature) to calculate an effective path length-concentration product, which can be used with the measured UV/visible absorbance to derive an extinction coefficient. The data from IR and UV/visible measurements on the same day and same sample were used. The visible absorption band was integrated and used (after accounting for the transition frequency) to derive an oscillator strength (f) of 0.022 for this transition. Using the $f=4.3\times10^{-9}\ \int\varepsilon(\bar{\nu})d\bar{\nu}$ equation,[81] where f is the calculated oscillator strength and ($\bar{\nu}$) is the energy (in wavenumbers), yields an ε_{max} of 2100 M^{-1} cm^{-1}.

In room-temperature solutions, the electronic absorption spectrum of *iso*-CF_2I_2 was captured by means of ultrafast transient absorption spectroscopy. The product absorption at 1 ns after 350 nm excitation of CF_2I_2 in CCl_4 consists of (i) absorption of ground-state I_2 (band centered at 518 nm) (ii) some minor contribution (<10%) from I_2 trapped in long-lived A/A' excited states [centered at 625 nm (Ref. 82)], and (iii) broad transient absorption between 350 and 490 nm. The short and intermediate time dynamics is reminiscent to that reported for CF_2I_2 in *n*-hexane, and the solvent effects through a series of chlorinated alkanes will be discussed

Downloaded 17 May 2010 to 134.48.30.80. Redistribution subject to AIP license or copyright; see http://jcp.aip.org/jcp/copyright.jsp

elsewhere. By subtracting the contribution of ground-state I_2 as well as contribution from I_2 (A/A') states, the product band can be discerned. The resulting band is broad, exhibiting an onset at around 500 nm followed by steeply rising absorption toward 450 nm and a weakly pronounced maximum at around 385 nm. This product spectrum can be assigned to the *iso*-CF_2I_2 isomer product based on the matrix isolation experiment. As shown in the lower panel of Fig. 5, the resulting 1 ns spectrum is virtually identical to the absorption spectrum of *iso*-CF_2I_2 trapped in the matrix isolation experiments [with subtracted $I_2(X)$ absorption[78]]. However, neither this absorption band nor 350 nm absorption were observed on a time scale of tens of nanosecond (20 ns) in nanosecond 350 nm pump/visible probe experiments. This indicates that the dark lifetime of the *iso*-CF_2I_2 species is shorter than 20 ns in room temperature CCl_4.

Based on the available experimental and computational data, several important conclusions can be drawn about the electronic structure of the *iso*-CF_2I_2 species, even though a rigorous description of the bonding and occupancies of relevant orbitals in the isomer requires further work and multireference *ab initio* calculations. Three types of structures are considered: (1) $D^{\cdots}I_2$, (2) D–I–I, and (3) $(D-I)^+-I^-$.[83] Structure (1) is a donor-acceptor complex, which for large enough D–I distances, can be viewed as a van der Waals complex (a sum of van der Waals radii of I and C atoms is 3.8 Å). A linear structure with a hypervalent (n-σ^*) I–I contact (so-called reverse ylide[84]) can be represented by (2). The I–I bond has ionic character in structure (3) for which the $[(D-I)^+]I^-$ salt is at the limit. Interestingly, the electronic absorption spectrum occurs in the visible range between 400 and 500 nm with $\varepsilon_{max} \sim 2100\ M^{-1}\ cm^{-1}$. Well-known electron donor-acceptor complexes of I_2 with ethers and alcohols exhibit comparable electronic absorption.[85] The calculated I–I stretch ($\nu_6 = 216\ cm^{-1}$) in *iso*-CF_2I_2 is deceivingly close to the I–I stretching fundamental in free I_2 ($212\ cm^{-1}$), but far from the I–I stretch in $D^{\cdots}I_2$ ($140-180\ cm^{-1}$ [83]). Both computational[86] and liquid-phase extended x-ray absorption fine structure (EXAFS)[87] studies show a slight increase [0.030 Å (Ref. 86) and 0.028 Å (Ref. 87)] of the I_2 bond length from the isolated I_2 molecule (2.66 Å) to the diethyl ether$^{\cdots}I_2$ complex. I–I bond distances ranging from 2.72 to 2.85 Å were found in other $D^{\cdots}I_2$ donor-acceptor complexes, where D=thioketones, phosphanes,[83] not close enough to the calculated I–I bond distance in *iso*-CF_2I_2 species (3.046 Å). On the other hand, the I–I distance is about 2.9 Å in (2) and more than 3.0 Å in (3).[83] The H_2C-I-I isomer of CH_2I_2 is bent along the C–I–I moiety (119.7°, CASPT2),[88] and its I–I bond distance is measured to be 3.02 Å,[22] consistent with important contributions from the $H_2C^+-X-Y^-$ (Refs. 3, 4, 17, and 18) and $H_2C-X^+-Y^-$ (Refs. 3, 4, and 18) resonance structures. However, this isomer species exhibits ε_{max} of $10^4\ M^{-1}\ cm^{-1}$ in matrices,[3,4] that is about fivefold larger than the ε_{max} of *iso*-CF_2I_2 in the same spectral range. As *iso*-CF_2I_2 is nearly axially symmetric, the value of ε_{max} may be small for symmetry reasons, as previously discussed for benzene$^{\cdots}I_2$ complexes.[89] The derived NBO and Mulliken charges reveal excess negative charge deposited on the outer iodine atom in the *iso*-CF_2I_2 isomer (and not on the central I-atom, as previously reported[41]), suggesting that the $F_2C-X^+-Y^-$ resonance structure contributes. This is also consistent with a small difference in vibrational frequencies for the C–I stretch mode in the F_2C-I-I isomer (Table II) and F_2C-I^+ radical cation[53] [Table S2 (Ref. 54)]. Therefore, the contribution of the $F_2C-X^+-Y^-$ ion-pair-like resonance structure to the total average wave-function is important, but it seems that a linear molecular structure of the isomer has important implications on its electronic structure and optical properties.

IV. CONCLUSIONS

The *iso*-CF_2I_2 (F_2C-I-I) intermediate, a weakly bound isomer of CF_2I_2, is trapped using the matrix isolation technique following UV irradiation of CF_2I_2 in cold Ar matrices. The first IR and visible spectra of *iso*-CF_2I_2 were obtained. Compared to the well-known isomers of dihalomethanes (CH_2IX, X=Cl Br, I), which exhibit characteristic dual absorption UV/visible bands, *iso*-CF_2I-I has a significantly different absorption spectrum. This implies that the electronic structure of the isomer is different, consistent with the difference in calculated geometric structures for *iso*-CF_2I-I, and, for example, *iso*-CH_2I-I. The assignment of the *iso*-CF_2I-I isomer was based on IR signatures correlated with calculated vibrational frequencies, and confirmed by annealing experiments. The formation of this isomer following UV excitation of CF_2I_2 in room temperature CCl_4 solutions was monitored by means of ultrafast time-resolved IR absorption through its intense CF_2 symmetric stretch. Furthermore, using the matrix isolation spectrum of *iso*-CF_2I-I and UV-visible transient absorption spectra for CF_2I_2 in CCl_4, the survival of a detectable amount of this intermediate on a 1 ns time scale following UV excitation of CF_2I_2 was also confirmed. Together, matrix isolation and ultrafast IR absorption experiments suggest that the formation of *iso*-CF_2I_2 occurs via recombination of CF_2I radical and I atom. In addition, ultrafast IR experiments detect a delayed population of the C–F stretching mode in *iso*-CF_2I-I, placing an upper limit of 400 fs for the primary C–I bond breaking and geminate recombination processes. The formation of this isomer in solution at room temperature has direct dynamic implications for the ultrafast production of molecular iodine from electronically excited CF_2I_2, a subject of future publications.

ACKNOWLEDGMENTS

A.N.T. thanks his BGSU colleagues James E. Yarnell for providing a ruthenium reference compound, Guifeng Li for assistance in IR measurements, and Ksenija D. Glusac for using the IR detection system, as well as Felix N. Castellano for using nanosecond flash photolysis equipment and Aaron A. Rachford for conducting the nanosecond experiments. A.N.T. gratefully acknowledges NSF CAREER award support (Grant No. CHE-0847707, A.N.T.). S.A.R. acknowledges support from the National Science Foundation (Grant No. CHE-0717960) and the donors of the Petroleum Research Fund of the American Chemical Society (Grant No. PRF 48740-ND6), and thanks Mario Fajardo and David Anderson for helpful advice concerning the matrix isolation

Downloaded 17 May 2010 to 134.48.30.80. Redistribution subject to AIP license or copyright; see http://jcp.aip.org/jcp/copyright.jsp

technique. P.Z.E. thanks Igor Schapiro and Massimo Olivucci for many useful discussions.

[1] A. H. Zewail, J. Phys. Chem. A **104**, 5660 (2000).
[2] A. N. Tarnovsky, J. L. Alvarez, A. P. Yartsev, V. Sundström, and E. Åkesson, Chem. Phys. Lett. **312**, 121 (1999).
[3] G. Maier, H. P. Reisenauer, J. Hu, L. J. Schaad, and B. A. Hess, J. Am. Chem. Soc. **112**, 5117 (1990).
[4] G. Maier and H. P. Reisenauer, Angew. Chem., Int. Ed. Engl. **25**, 819 (1986).
[5] X. M. Zheng and D. L. Phillips, J. Phys. Chem. A **104**, 6880 (2000).
[6] W. M. Kwok, C. Ma, A. W. Parker, D. Phillips, M. Towrie, P. Matousek, and D. L. Phillips, J. Chem. Phys. **113**, 7471 (2000).
[7] X. Zheng and D. L. Phillips, Chem. Phys. Lett. **324**, 175 (2000).
[8] A. N. Tarnovsky, M. Wall, M. Gustafsson, N. Lascoux, V. Sundström, and E. Åkesson, J. Phys. Chem. A **106**, 5999 (2002).
[9] X. Zheng, W.-H. Fang, and D. L. Phillips, J. Chem. Phys. **113**, 10934 (2000).
[10] W. Ming Kwok, C. Ma, D. Phillips, A. W. Parker, M. Towrie, P. Matousek, and D. Lee Phillips, Chem. Phys. Lett. **341**, 292 (2001).
[11] X. Zheng and D. L. Phillips, J. Chem. Phys. **113**, 3194 (2000).
[12] H. Ihee, M. Lorenc, T. K. Kim, Q. Y. Kong, M. Cammarata, J. H. Lee, S. Bratos, and M. Wulff, Science **309**, 1223 (2005).
[13] C. Grimm, A. Kandratsenka, P. Wagener, J. Zerbs, and J. Schroeder, J. Phys. Chem. A **110**, 3320 (2006).
[14] A. N. Tarnovsky, M. Wall, M. Rasmusson, T. Pascher, and E. Åkesson, J. Chin. Chem. Soc. (Taipei) **47**, 769 (2000).
[15] C. E. Jones and L. J. Carpenter, Environ. Sci. Technol. **39**, 6130 (2005).
[16] D. L. Phillips, W. H. Fang, X. Zheng, Y. L. Li, D. Wang, and W. M. Kwok, Curr. Org. Chem. **8**, 739 (2004).
[17] D. L. Phillips, W.-H. Fang, and X. Zheng, J. Am. Chem. Soc. **123**, 4197 (2001).
[18] A. N. Tarnovsky, V. Sundström, E. Åkesson, and T. Pascher, J. Phys. Chem. A **108**, 237 (2004).
[19] M. Kawasaki, S. J. Lee, and R. Bersohn, J. Chem. Phys. **63**, 809 (1975).
[20] P. M. Kroger, P. C. Demou, and S. J. Riley, J. Chem. Phys. **65**, 1823 (1976).
[21] W. M. Kwok, C. Ma, A. W. Parker, D. Phillips, M. Towrie, P. Matousek, X. Zheng, and D. L. Phillips, J. Chem. Phys. **114**, 7536 (2001).
[22] J. Davidsson, J. Poulsen, M. Cammarata, P. Georgiou, R. Wouts, G. Katona, F. Jacobson, A. Plech, M. Wulff, G. Nyman, and R. Neutze, Phys. Rev. Lett. **94**, 245503 (2005).
[23] J. Vincent, M. Andersson, M. Eklund, A. B. Wohri, M. Odelius, E. Malmerberg, Q. Y. Kong, M. Wulff, R. Neutze, and J. Davidsson, J. Chem. Phys. **130**, 154502 (2009).
[24] M. Wall, A. N. Tarnovsky, T. Pascher, V. Sundström, and E. Åkesson, J. Phys. Chem. A **107**, 211 (2003).
[25] A. N. Tarnovsky, I. Pascher, and T. Pascher, J. Phys. Chem. A **111**, 11814 (2007).
[26] P. Z. El-Khoury, W. M. Kwok, X. G. Guan, C. S. Ma, D. L. Phillips, and A. N. Tarnovsky, ChemPhysChem **10**, 1895 (2009).
[27] W. M. Kwok, C. Zhao, Y.-L. Li, X. Guan, D. Wang, and D. L. Phillips, J. Am. Chem. Soc. **126**, 3119 (2004).
[28] X. G. Guan, X. F. Lin, W. M. Kwok, Y. Du, Y. L. Li, C. Y. Zhao, D. Q. Wang, and D. L. Phillips, J. Phys. Chem. A **109**, 1247 (2005).
[29] W. M. Kwok, C. S. Ma, A. W. Parker, D. Phillips, M. Towrie, P. Matousek, and D. L. Phillips, J. Phys. Chem. A **107**, 2624 (2003).
[30] G. Baum, P. Felder, and J. R. Huber, J. Chem. Phys. **98**, 1999 (1993).
[31] K. Bergmann, R. T. Carter, G. E. Hall, and J. R. Huber, J. Chem. Phys. **109**, 474 (1998).
[32] E. A. J. Wannenmacher, P. Felder, and J. R. Huber, J. Chem. Phys. **95**, 986 (1991).
[33] W. G. Roeterdink and M. H. M. Janssen, J. Chem. Phys. **117**, 6500 (2002).
[34] H. A. Scheld, A. Furlan, and J. R. Huber, Chem. Phys. Lett. **326**, 366 (2000).
[35] P. Farmanara, V. Stert, H. H. Ritze, and W. Radloff, J. Chem. Phys. **113**, 1705 (2000).
[36] W. Radloff, P. Farmanara, V. Stert, E. Schreiber, and J. R. Huber, Chem. Phys. Lett. **291**, 173 (1998).
[37] P. Z. El-Khoury and A. N. Tarnovsky, Chem. Phys. Lett. **453**, 160 (2008).
[38] X. M. Zheng and D. L. Phillips, Chem. Phys. Lett. **316**, 524 (2000).
[39] X. M. Zheng and D. L. Phillips, Chem. Phys. Lett. **313**, 467 (1999).
[40] P. Z. El-Khoury, A. N. Tarnovsky, I. Schapiro, M. N. Ryazantsev, and M. Olivucci, J. Phys. Chem. A **113**, 10767 (2009).
[41] P. Z. El-Khoury, M. Olivucci, and A. N. Tarnovsky, Chem. Phys. Lett. **462**, 192 (2008).
[42] M. N. Glukhovtsev and R. D. Bach, Chem. Phys. Lett. **269**, 145 (1997).
[43] M. M. Rochkind, Anal. Chem. **39**, 567 (1967).
[44] R. N. Perutz and J. J. Turner, J. Chem. Soc., Faraday Trans. 2 **69**, 452 (1973).
[45] L. J. Allamandola, D. Lucas, and G. C. Pimentel, Rev. Sci. Instrum. **49**, 913 (1978).
[46] A. Thoma, B. E. Wurfel, R. Schlacta, G. M. Lask, and V. E. Bondebey, J. Phys. Chem. **96**, 7231 (1992).
[47] Y. Zhao and D. G. Truhlar, Theor. Chem. Acc. **120**, 215 (2008).
[48] K. A. Peterson, B. C. Shepler, D. Figgen, and H. Stoll, J. Phys. Chem. A **110**, 13877 (2006).
[49] A. J. Sadlej, Theor. Chim. Acta **81**, 339 (1992).
[50] M. J. Frisch, G. W. Trucks, H. B. Schlegel *et al.*, GAUSSIAN 09, Gaussian Inc., Wallingford, CT, 2009.
[51] D. E. Milligan and M. E. Jacox, J. Chem. Phys. **48**, 2265 (1968).
[52] D. E. Milligan, D. E. Mann, M. E. Jacox, and R. A. Mitsch, J. Chem. Phys. **41**, 1199 (1964).
[53] F. T. Prochaska and L. Andrews, J. Am. Chem. Soc. **100**, 2102 (1978).
[54] See supplementary material at http://dx.doi.org/10.1063/1.3357728 for the supplementary figures.
[55] W. H. Fang, D. L. Phillips, D. Q. Wang, and Y. L. Li, J. Org. Chem. **67**, 154 (2002).
[56] Q. Y. Kong, M. Wulff, S. Bratos, R. Vuilleumier, J. Kim, and H. Ihee, J. Phys. Chem. A **110**, 11178 (2006).
[57] Q. Y. Kong, M. Wulff, J. H. Lee, S. Bratos, and H. Ihee, J. Am. Chem. Soc. **129**, 13584 (2007).
[58] J. H. Lee, J. Kim, M. Cammarata, Q. Kong, K. H. Kim, J. Choi, T. K. Kim, M. Wulff, and H. Ihee, Angew. Chem., Int. Ed. **47**, 1047 (2008).
[59] J. H. Lee, T. K. Kim, J. Kim, Q. Kong, M. Cammarata, M. Lorenc, M. Wulff, and H. Ihee, J. Am. Chem. Soc. **130**, 5834 (2008).
[60] C. Tao, C. Mukarakate, Y. Mishchenko, D. Brusse, and S. A. Reid, J. Phys. Chem. A **111**, 10562 (2007).
[61] C. Tao, C. Mukarakate, and S. A. Reid, J. Am. Chem. Soc. **128**, 9320 (2006).
[62] J. Kim, S. Jun, J. Kim, and H. Ihee, J. Phys. Chem. A **113**, 11059 (2009).
[63] C. G. Elles and F. F. Crim, Annu. Rev. Phys. Chem. **57**, 273 (2006).
[64] K. Iwata and H. O. Hamaguchi, J. Phys. Chem. A **101**, 632 (1997).
[65] J. C. Owrutsky, D. Raftery, and R. M. Hochstrasser, Annu. Rev. Phys. Chem. **45**, 519 (1994).
[66] T. Elsaesser and W. Kaiser, Annu. Rev. Phys. Chem. **42**, 83 (1991).
[67] G. Angel, R. Gagel, and A. Laubereau, Chem. Phys. Lett. **156**, 169 (1989).
[68] C. G. Elles, D. Bingemann, M. M. Heckscher, and F. F. Crim, J. Chem. Phys. **118**, 5587 (2003).
[69] H. J. Bakker, P. C. M. Planken, and A. J. Langendijk, J. Chem. Phys. **94**, 6007 (1991).
[70] A. Charvat, J. Assmann, B. Abel, and D. Schwarzer, J. Phys. Chem. A **105**, 5071 (2001).
[71] M. Rini, A. Kummrow, J. Dreyer, E. T. J. Nibbering, and T. Elsaesser, Faraday Discuss. **122**, 27 (2003).
[72] P. Hamm, S. M. Ohline, and W. Zinth, J. Chem. Phys. **106**, 519 (1997).
[73] V. Lehtovuori, J. Aumanen, P. Myllyperkio, M. Rini, E. T. J. Nibbering, and J. Korppi-Tommola, J. Phys. Chem. A **108**, 1644 (2004).
[74] J. Lindner, D. Cringus, M. S. Pshenichnikov, and P. Vöhringer, Chem. Phys. **341**, 326 (2007).
[75] K. Heyne, G. M. Krishnan, and O. Kühn, J. Phys. Chem. B **112**, 7909 (2008).
[76] V. M. Kenkre, A. Tokmakoff, and M. D. Fayer, J. Chem. Phys. **101**, 10618 (1994).
[77] Z. Wang, A. Pakoulev, and D. D. Dlott, Science **296**, 2201 (2002).
[78] L. Andrews, E. S. Prochaska, and A. Loewenschuss, Inorg. Chem. **19**, 463 (1980).
[79] S. Koda, J. Phys. Chem. **83**, 2065 (1979).
[80] S. Koda, Chem. Phys. Lett. **55**, 353 (1978).
[81] N. J. Turro, *Modern Molecular Photochemistry* (The Benjamin/Cummings, Menlo Park, CA, 1978).
[82] A. L. Harris, M. Berg, and C. B. Harris, J. Chem. Phys. **84**, 788 (1986).
[83] P. Deplano, J. R. Ferraro, M. L. Mercuri, and E. F. Trogu, Coord. Chem. Rev. **188**, 71 (1999).

Downloaded 17 May 2010 to 134.48.30.80. Redistribution subject to AIP license or copyright; see http://jcp.aip.org/jcp/copyright.jsp

[84] W. Kirmse, Eur. J. Org. Chem. 2005, 237.
[85] R. S. Mulliken, J. Am. Chem. Soc. **72**, 600 (1950).
[86] S. S. C. Ammal, S. P. Ananthavel, J. Chandrasekhar, P. Venuvanalingam, and M. S. Hegde, Chem. Phys. Lett. **248**, 153 (1996).
[87] U. Buontempo, A. DiCicco, A. Filipponi, M. Nardone, and P. Postorino, J. Chem. Phys. **107**, 5720 (1997).
[88] Y. J. Liu, L. De Vico, R. Lindh, and W. H. Fang, ChemPhysChem **8**, 890 (2007).
[89] F. C. Grozema, R. W. J. Zijlstra, M. Swart, and P. T. v. Duijnen, Int. J. Quantum Chem. **75**, 709 (1999).

Downloaded 17 May 2010 to 134.48.30.80. Redistribution subject to AIP license or copyright; see http://jcp.aip.org/jcp/copyright.jsp